J Appl Electrochem (2010) 40:23–28
DOI 10.1007/s10800-009-9959-2

ORIGINAL PAPER

Electrochemical and structural characterization of copper recycled from anodes of spent Li-ion batteries

V. G. Celante · M. K. Pietre · M. B. J. G. Freitas

Received: 1 April 2009 / Accepted: 9 June 2009 / Published online: 25 June 2009

Abstract In this study, the charge efficiency, nucleation growth, and morphology of electrodeposited copper from spent Li-batteries were studied. The charge efficiency for these deposits shows a maximum value of 99.41%, under a charge density of 5.0 C cm^{-2}. Studies with the SEM technique at pH 2.0 show well-formed nuclei. At pH 4.5, the deposits take the form of dendrites. XRD analysis shows that, in both cases, a Cu_2O structure is present, but with a large amount at pH 4.5, evidenced by peaks of [002] and [110] directions.

Keywords Li-ion batteries · Recycling · Copper · Electrodeposition

1 Introduction

In the period between 2000 and 2008, the annual production of Li-ion batteries increased by 800% and it is predicted to increase even more next years [1] due to the higher power density of Li-ion batteries in comparison to other secondary batteries, like Ni-Cd and Ni-MH [2]. Because Li-ion batteries are composed of valuable metals and components, like cobalt, copper, and electrolyte solution, the recycling process has become important in as the concern for an environment free of toxic components increases [3]. For recycling copper from the current collector for the negative electrode, some processes can be related, such as: precipitation, extraction, or electrodeposition [4, 5]. One of these is the electrochemical process where electrodeposition baths are made, with or without the addition of complexing additives to increase efficiency. An important characteristic of these electrodeposits is the morphology, where the electrodeposit growth can be related to the nucleation process (in two or three dimensions). Searson et al. [6] studied the morphology and kinetics for copper nucleation during electrodeposition in strongly acid media (pH ~1.0) without additives. They observed that copper electrodeposition occurs at potentials over −0.04 V and consists of the direct reduction of Cu^{2+} to metallic copper. With in situ analysis, they also observed that the current increases at slower rates related to the decrease in the quantity of ions from the bulk to the interface, showing a diffusion/reaction-controlled process. For more negative potentials, the growth of nuclei was controlled by diffusion. Zangari et al. [7] observed that, at pH 2.5, the copper morphology shows a dendritic form and then forms clusters of electrodeposit. Pesic and Grujicic [8] correlated the nucleation process of copper electrodeposition and morphology and observed that, at pH values over 3, the nucleation process was progressive (three-dimensional growth) and, below this value, the model tended to an instantaneous nucleation, related to a bi-dimensional growth. Pasquale et al. [9] studied the morphology of copper electrodeposits. They observed that the bath composition (preferably pH values) has a significant influence on the copper morphology, with well-formed grains and nuclei being formed in acid media. Otherwise, at higher pH values, Gabrielli et al. [10] observed that copper electrodeposition formed small dendrites related to a copper metallic layer and another oxide layer, normally Cu_2O. Nikolitic et al. [11] observed that the hydrogen co-deposition with metallic copper was related to a three-dimensional growth due to the porous morphology. In this study, the nucleation process, morphology and structure of copper

V. G. Celante · M. K. Pietre · M. B. J. G. Freitas (✉)
Departamento de Química, Laboratório de Eletroquímica Aplicada, Universidade Federal do Espírito Santo, Av. Fernando Ferrari 514, Goiabeiras, Vitória-ES CEP: 29075-910, Brazil
e-mail: marcosbj@hotmail.com

recycled from the current collector of Li-ion batteries were studied. The relationship between the Scharifker–Hills nucleation model and structure was observed by the correlation of the potentiostatic technique and analysis of scanning electronic microscopy (SEM), X-ray diffractometry (XRD), and energy dispersive scanning (EDS).

2 Experimental procedure

2.1 Preparation of electrodeposition solutions

Spent Li-ion batteries were physically dismantled and separated into their different parts: anode, cathode, organic separators, steel compartment, and current collectors. The negative electrode (copper + carbon material) was separated. This material was dried in air at 120 °C for 24 h to evaporate organic compounds present in the electrolyte solution, such as ethylene carbonate (EC) and propylene carbonate (PC). The current collector was also separated from the active material. The copper current collector was then washed with distilled water at 40 °C to eliminate lithium salts also present in the electrolyte. A mass of 9.21 g of current collector was dissolved in a solution containing 470.00 mL of 3.00 mol L^{-1} H_2SO_4, and 30.00 mL of 30% v/v H_2O_2, and the system was kept under magnetic stirring at 60 °C for 2 h. The addition of H_2O_2 is necessary to increase the efficiency of copper dissolution, since copper is partially insoluble in H_2SO_4 solutions. The carbon active material was separated by filtration from the leaching solution. All experimental procedures can be seen in Fig. 1. Equation 1 shows the entire process:

$$Cu_{(s)} + H_2SO_{4(aq)} + H_2O_{2(aq)} \rightarrow CuSO_{4(aq)} + 2H_2O_{(l)} \quad (1)$$

The pH of the leaching solution was adjusted with KOH pellets to 2.0 or 4.5. The solutions were buffered with 0.10 mol L^{-1} H_3BO_3, and 0.5 mol L^{-1} K_2SO_4 was added as a supporting electrolyte. The ionic copper concentration in the baths was equal to 0.00098 mol L^{-1}, as measured by Inductively Coupled Plasma Mass Spectroscopy (ICP-MS). The copper solution was submitted to a nitrogen flux for 30.0 min to eliminate the presence of oxygen.

2.2 Electrochemical measures

Potentiostatic and potentiodynamic experiments were performed in an AUTOLAB PGSTAT 100 with an electrochemical impedance spectroscopy (EIS) module. The working electrode was Al 98% MERCK (0.25 cm^2). The counter electrode was made of graphite (3.00 cm^2) and the reference electrode was Ag/AgCl/KCl saturated.

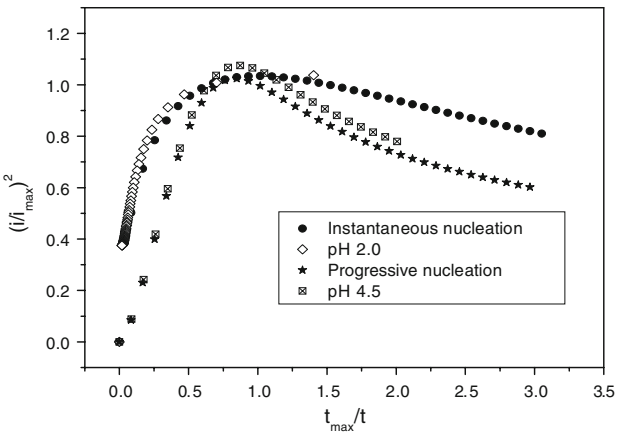

Fig. 1 Nucleation models for electrodeposited copper, applied potential $E = -0.3$ V, $[Cu^{2+}] = 0.001$ mol L^{-1}, and H_3BO_3 as buffer, and 0.5 mol L^{-1} K_2SO_4 as a supporting electrolyte

DRX analysis was performed in a Shimadzu CRD 7000 diffractometer, at room temperature, with Cu Kα radiation, 40.0 kV, 30.0 mA, and 2.00 min^{-1}. The diffractograms were obtained in $2\theta = 5.00$–$50.0°$. SEM and EDS analysis were performed in a JEOL 6360LV microscope, with previous covering with carbon in a Bal-Tec MED020 vaporizer, with a NoranSystem Six spectrophotometer coupled to the microscope.

3 Results and discussion

3.1 Nucleation mechanism

Figure 1 shows the nucleation models applied to copper electrodeposition onto the aluminum substrate working electrode, at both pH values under potentiostatic deposition at −0.3 V. The Scharifker and Hills models can be seen in Eq. 2 for instantaneous nucleation and Eq. 3 for progressive nucleation. At pH 2.0, an instantaneous nucleation mechanism is observed. In this case, the nuclei growth is simultaneous to the nucleation mechanism, leading to a large amount of small nuclei. At pH 4.5, the deposition tends to favor a progressive nucleation, with large nuclei formed and a three-dimensional growth being observed.

$$\frac{i^2}{i_{max}^2} = 1{,}9542\left(\frac{t_{max}}{t}\right)\left[1 - \exp\left(-1{,}2564\frac{t}{t_{max}}\right)\right]^2 \quad (2)$$

$$\frac{i^2}{i_{max}^2} = 1{,}2254\left(\frac{t_{max}}{t}\right)\left[1 - \exp\left(-2{,}3367\frac{t^2}{t_{max}^2}\right)\right]^2 \quad (3)$$

3.2 Crystallization overpotential

One of the most important electrochemical parameters in an electrodeposition process is the crystallization

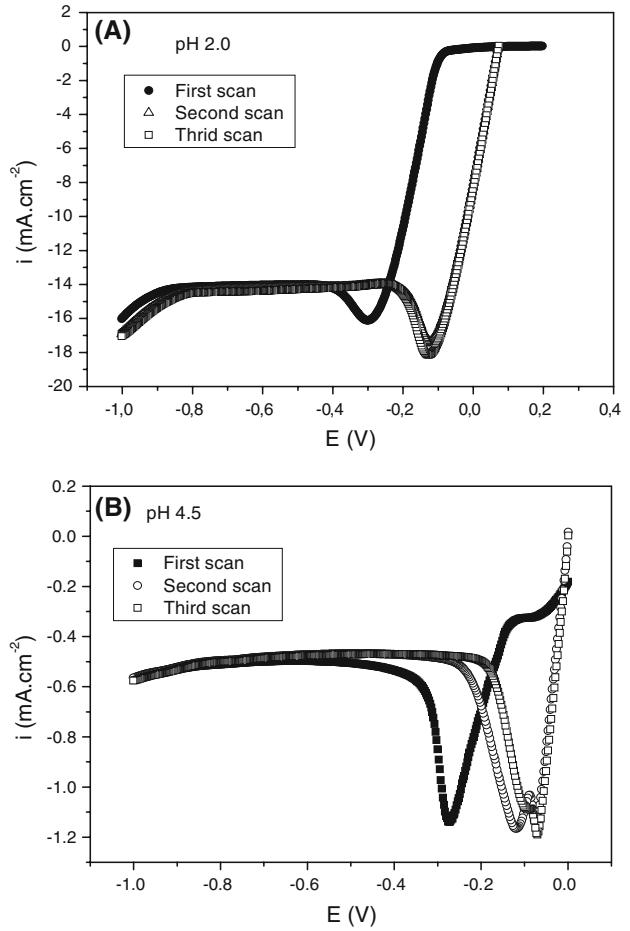

Fig. 2 Successive scans for copper electrodeposition in pH 2.0 and 4.5, $[Cu^{2+}] = 0.001$ mol L^{-1} and H_3BO_3 as buffer, and 0.5 mol L^{-1} K_2SO_4 as a supporting electrolyte, $v = 10$ mV s^{-1}

overpotential. Figure 2a and b shows the successive scans in copper electrodeposition at pH 2.0 and 4.5 onto an aluminum electrode. In the first scan, the cathodic peak related to copper reduction appears at −0.366 V as a single peak, suggesting a one-step process in the direct reduction of Cu^{2+} to metallic copper. In the second and third scans, the cathodic peak appears at −0.150 V. Therefore, the overpotential of the Cu–Cu interaction is lower than the overpotential of the Cu–Al interaction. This suggests that the energy necessary to electrodeposit copper onto an aluminium substrate is higher than the energy to electrodeposit copper onto a copper layer already deposited. Figure 2b shows the same experiment of electrocrystallization from a solution at pH 4.5. As before, the overpotential for Cu electrodeposition onto Cu is lower than for Cu onto Al and the same considerations can be made. However, is this case, two cathodic peaks can be seen and are related to the quick passage of Cu^{2+} to Cu^{+} (−0.083 V) and to the electrodeposition of metallic copper in the reaction of Cu^{+} to Cu (−0.146 V).

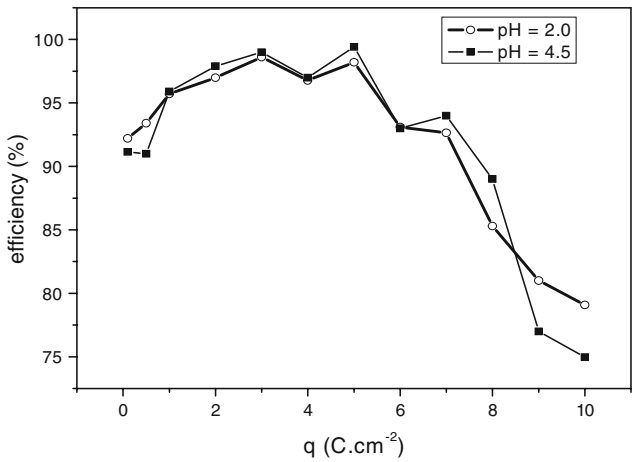

Fig. 3 Charge efficiency vs. charge applied for copper electrodeposition with $[Cu^{2+}] = 0.001$ mol L^{-1} and H_3BO_3 as buffer, and 0.5 mol L^{-1} K_2SO_4 as a supporting electrolyte

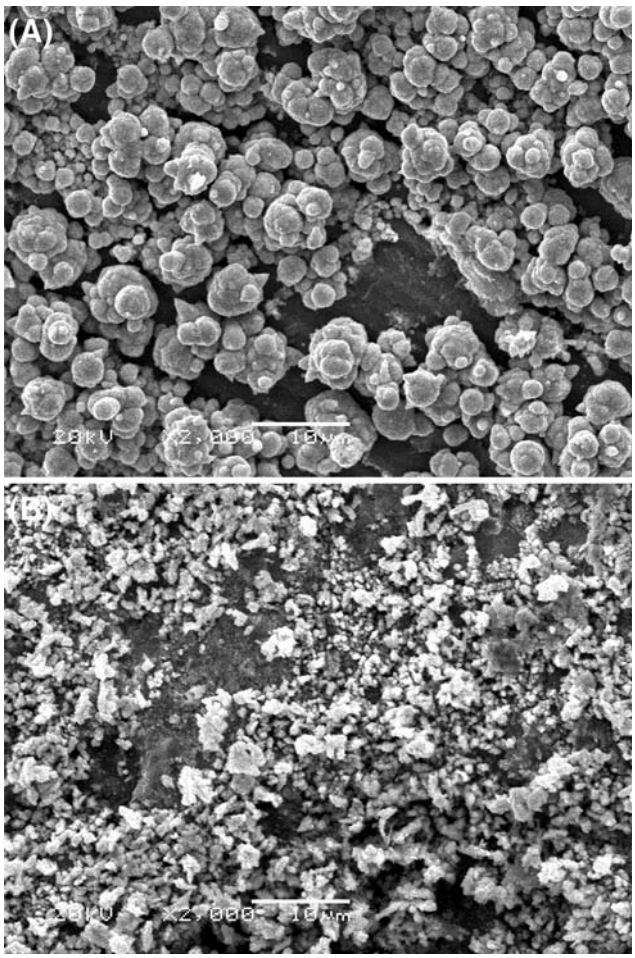

Fig. 4 SEM for copper electrodeposition, applied potential $E = -0.3$ V, $[Cu^{2+}] = 0.001$ mol L^{-1}, H_3BO_3 0.1 mol L^{-1} as buffer, and 0.5 mol L^{-1} K_2SO_4 as a supporting electrolyte, 5.0 C cm^{-2}, 2000×; **a** pH = 2.0 and **b** pH = 4.5

3.3 Charge efficiency, and SEM of copper electrodeposits

Experiments were accomplished to study the influence of the charge density and solution pH on the morphology of copper electrodeposits. In order to analyze the efficiency of the ionic copper electrodeposition, different charge densities were applied and maintained at a potential of −0.30 V. The charge efficiency was analyzed in Fig. 3 from C cm^{-2} 0.1 to 10.0 C cm^{-2}. A maximum efficiency of 95–98% was obtained in the interval of charge density between 3.0 and 5.0 C cm^{-2} for both pH conditions. This high efficiency shows a decrease in possible parallel reactions, such as the detachment of hydrogen. The efficiency decrease occurs because the ionic copper concentration in solution decreases with the increase in charge density.

Copper electrodeposits obtained at a potential of −0.3 V, with 3.0 and 5.0 C cm^{-2}, were analyzed by the SEM technique. Figure 4 shows the SEM image of copper electrodeposited at pH 2.0 and 4.5, respectively. As can be seen in Fig. 4a, the copper electrodeposited from a solution with a pH equal to 2.0 presents large macrospores. The progressive growth or 3D mechanism to growth with formation of large nuclei in small quantities is favored at pH 2.0. As a result of this preferential growth, the mechanism of copper morphology presents macrospores. As can be seen in Fig. 4b, the deposit surface is more regular and reduces the presence of macroporosity. The copper nuclei were well formed and a smaller size than at pH 2.0. The formation and growth of the electrodeposits tend towards a simultaneous two and three-dimensional process. The deposits are very irregular and present holes (areas without deposition).

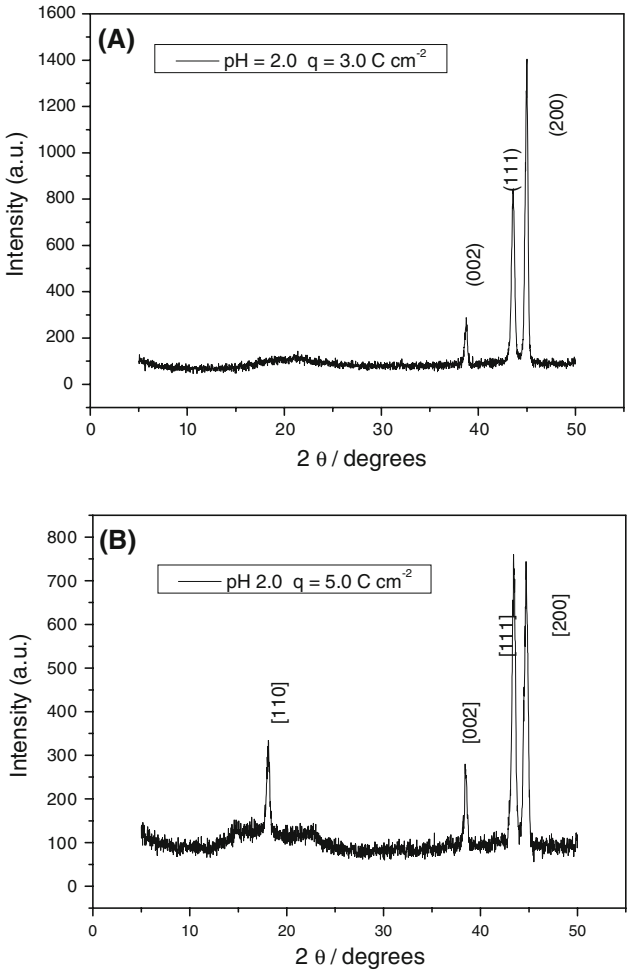

Fig. 5 The X-ray diffractograms for electrodeposited copper, applied potential $E = -0.3$ V, $[Cu^{2+}] = 0.001$ mol L^{-1}, pH = 2.0, **a** $q = 3.0$ C cm^{-2} and **b** $q = 5.0$ C cm^{-2}, H_3BO_3 0.1 mol L^{-1} as buffer

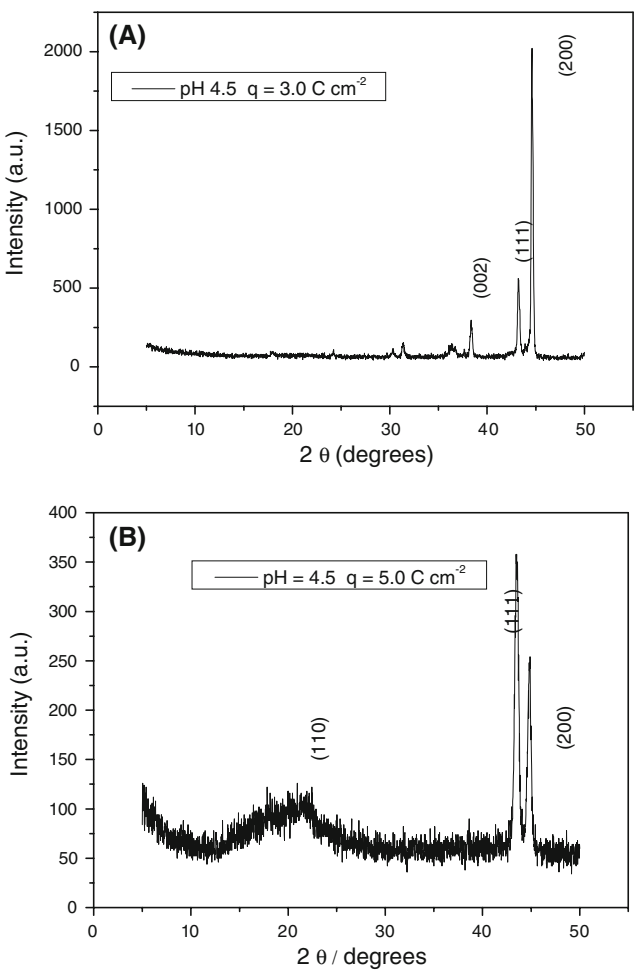

Fig. 6 The X-ray diffractograms for electrodeposited copper, applied potential $E = -0.3$ V, $[Cu^{2+}] = 0.001$ mol L^{-1}, pH = 4.5, **a** $q = 5.0$ C cm^{-2}, **b** $q = 5.0$ C cm^{-2}, and H_3BO_3 0.1 mol L^{-1} as buffer

3.4 X-ray diffraction, and EDS analysis of cobalt electrodeposits

The XRD analysis, in Fig. 5a (3.0 C cm^{-2}) and b (5.0 C cm^{-2}) at pH 2.0, shows that the peaks corresponding to directions [111] and [200] are characteristic of an fcc structure for electrodeposited copper, according to the Joint Committee on Powder Diffraction Standards (JCPDS) [12]. Direction [002] is related to the Cu_2O structure [13]. An increase in the charge density leads to poor crystallinity, with the presence of the [110] direction, which is also related to Cu_2O. The XRD results for copper electrodeposited at pH 4.5 are shown in Fig. 6a (3.0 C cm^{-2}) and b (5.0 C cm^{-2}) and have a similar pattern when compared with those shown in Fig. 5. The peaks for fcc structure in the [111], [200], and [002] directions are present. Also in this case, the intensity of the [200] peak decreases with an increase in the charge density. This result leads to an observation that, at pH 2.0, copper tends to electrodeposit in a preferential 3D structure and, at pH 4.5, it tends to deposit in a 2D structure. Simultaneous growth can be observed in both cases with an increase in the charge density. Figure 7 presents a typical EDS analysis (3.0 C cm^{-2}) at pH 2.0 and 4.5. In the EDS plots, it can be see that the surface is mostly covered by copper and oxygen.

3.5 Potentiodynamic dissolution of copper electrodeposits

The electrodissolution of copper electrodeposits was performed with an Al working electrode as a substrate, at different charge densities in 0.5 mol L^{-1} H_2SO_4 solution. In Fig. 8a, the dissolution of copper deposits with $q = 3.0$ C cm^{-2} shows a two-step process, evidenced by the two peaks. The first one, marked **I**, is related to Cu^+ formation in the structure of Cu_2O. This can already be seen by DRX in the peaks of the [002] and [110] directions. With an increase in the potential, the region responsible for Cu^+ is quickly suppressed and turns to Cu^{2+} with peaks of DRX related to directions [111] and [200], passing to

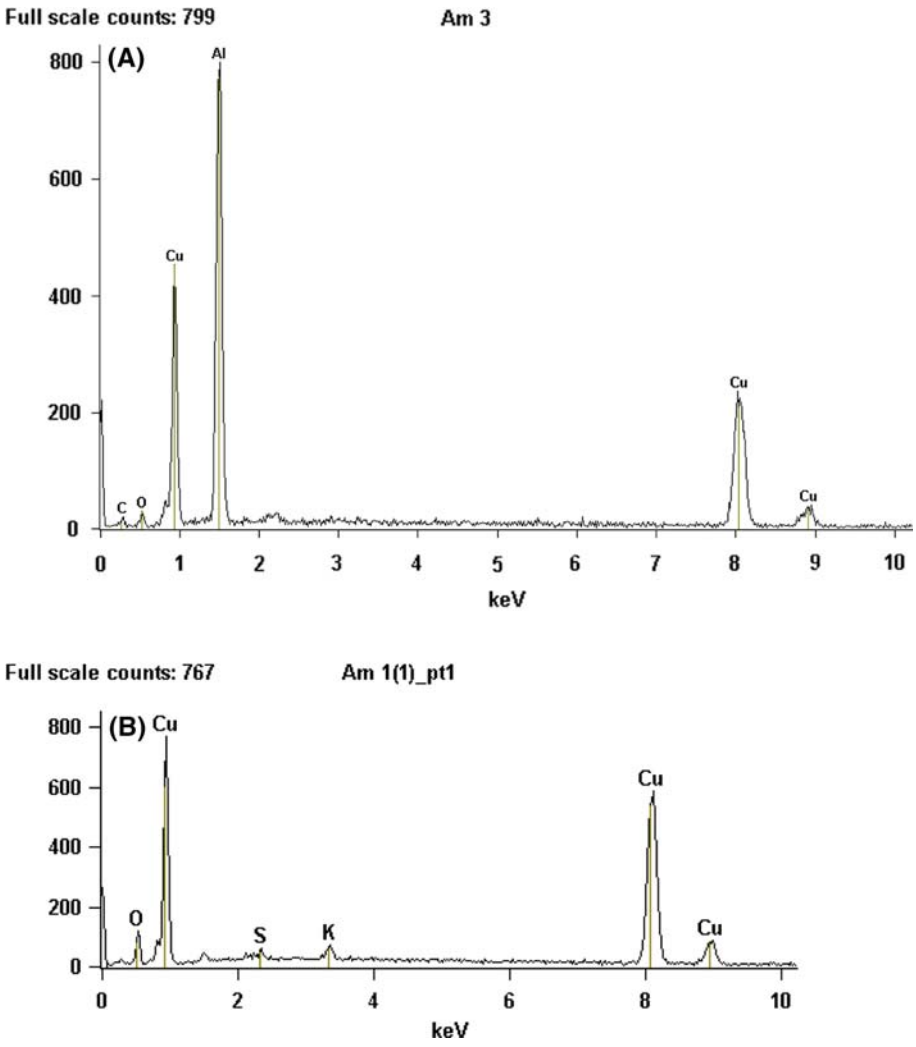

Fig. 7 EDS for copper electrodeposition, applied potential $E = -0.3$ V, $[Cu^{2+}] = 0.001$ mol L^{-1}, 3.0 C cm^{-2}, **a** pH = 2.0 and **b** 4.5 C cm^{-2}

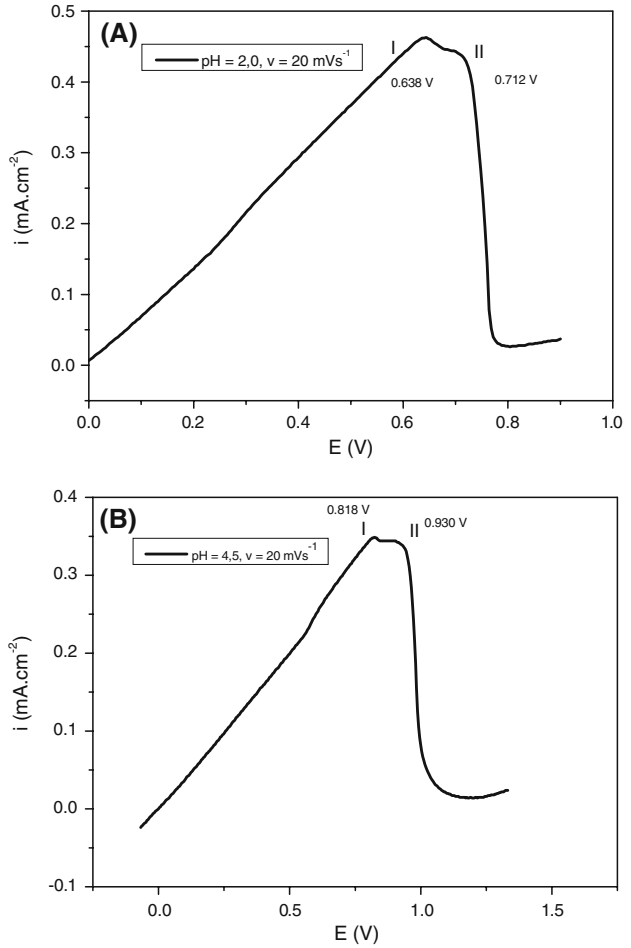

Fig. 8 Potentiodynamic dissolution of copper with $[Cu^{2+}] = 0.001$ mol L^{-1}, $q = 3.0$ C cm^{-2} and H_3BO_3 0.1 mol L^{-1} as buffer, $v = 10$ mV s^{-1}, **a** pH 2.0 and **b** pH 4.5

complete dissolution of the electrodeposit. Figure 8b shows a similar result at pH 4.5, with the region of Cu^{+} quickly turned to Cu^{2+} to complete dissolution. The efficiency of dissolution in these electrodeposits shows that, at a charge density of 3.0 C cm^{-2} at both pH values, the efficiency was 97.63% (pH 2.0) and 94.16% (pH 4.5). For a charge density equal to 5.0 C cm^{-2}, the efficiency decreased to 89.70% (pH 2.0) and 61.01% (pH 4.5). This result can again be related to the fact that, at a high charge density, the copper oxide layer is formed in greater quantity than at a charge density of 3.0 C cm^{-2}.

4 Conclusions

The mechanism of copper electrodeposition shows a step where the intermediate Cu^{+} is present, according to potentiodynamic experiments, in both pH cases. At pH 4.5, this intermediate has a substantial influence. The dissolution shows that, at pH 2.0, almost 100% of the electrodeposit is dissolved and, at pH 4.5, there is a resistive layer of Cu_2O that does not dissolve. The charge efficiency shows results over 90% for copper electrodeposition in both cases. The XRD, SEM, and EDS analyses show that the [200] direction is related to 3D-growth and the [111] direction to 2D-growth. At pH 2.0, 3D-growth was found in almost total quantity and, at pH 4.5, there was 2D-growth. In both cases, a simultaneous 2D- and 3D-growth was found with an increase in charge density. The peaks in the [110] and [002] directions were related to the Cu_2O structure. The electrodeposits were formed mostly by Cu, and, at pH 4.5, there was a small quantity of oxygen.

Acknowledgments The authors acknowledge MCT-CNPq-FAPES process number 36303542/2007.

References

1. Cobalt Development Institute (2005) In: Cobalt News. http://www.thecdi.com. Accessed 14 Apr 2007
2. Takeno K, Takano K et al (2005) J Power Sources 298:305
3. Castillo S, Ansart F et al (2002) J Power Sources 247:254
4. Aurbach D, Markovisky B et al (2007) J Power Sources 491:499
5. Xu J, Thomas HR et al (2008) J Power Sources 512:527
6. Searson PC, Ross FM et al (2006) Surf Sci 1817:1826
7. Zangari G, Arrington D et al (2008) Electrochim Acta 2644:2649
8. Pesic B, Grujicic D (2002) Electrochim Acta 2901:2912
9. Pasquale MA, Gassa LM et al (2008) Electrochim Acta 5891:5904
10. Gabrielli C, Devos O et al (2007) J Electroanal Chem 95:102
11. Nikolitic ND, Brankovic G et al (2008) J Electroanal Chem 13:21
12. Joint Committee on Powder Diffraction Standards (1991) Diffraction Data File, No.45-0594, JCPDS international center for diffraction data, Pennsylvania
13. Joint Committee on Powder Diffraction Standards (1991) Diffraction Data File, No.5-661, JCPDS international center for diffraction data, Pennsylvania